Implementation of Flat Gain Broadband Power Amplifier With Impedance Rotation Compensation

XIANGYU MENG[1], **CUIPING YU**[2], **YUANAN LIU**[2], **(Member, IEEE)**,
YONGLE WU[2], **(Senior Member, IEEE), XIYU WANG**[3], **AND JIANWEI WANG**[3]

[1]The ZTE Corporation of China, Shenzhen 518057, China
[2]Beijing Key Laboratory of Work Safety Intelligent Monitoring, Department of Electronic Engineering, Beijing University of Posts and Telecommunications, Beijing 100876, China
[3]State Key Laboratory of Mobile Network and Mobile Multimedia Technology, The ZTE Corporation of China, Shenzhen 518057, China

Corresponding author: Cuiping Yu (yucuiping@bupt.edu.cn)

ABSTRACT The conventional broadband impedance matching network in low-pass structure cannot present adequate broadband impedance rotation for the optimum broadband operation of the power amplifier (PA), resulting in performance variations and degradations. The underlying constraint is the phenomenon of opposite impedance rotation. Against such a backdrop, this paper presents a methodology using the band-pass topology to compensate the frequency-variable response of the PA. The CGH40010F from Cree is used to verify the effectiveness of this compensation method. The experimental results are in good agreement with the simulation. The proposed PA yields good gain flatness (± 0.5 dB), input/output return loss (>13 dB), and high power added efficiency (>60 %) over the band from 1.7 to 2.7 GHz. After digital predistortion, the measured adjacent channel power ratio is about -55 and -50 dBc at ± 5 and ± 10 MHz offset when the PA is driven by 5- and 10-MHz WCDMA signals at $6.5 \sim 7$ dB power back-off.

INDEX TERMS Band-pass matching network, broadband impedance rotation, broadband reactive matching, power amplifier, synthesis method.

I. INTRODUCTION

Modern wireless devices and subsystems for current 4G, approaching 5G and beyond are expected to provide several mobile accesses, resulting co-existence of multiple telecommunication protocols and operations at bands that are widely separated in frequency. Meanwhile, the carrier aggregation (CA), one of main techniques in current and new coming mobile communications, reveals that mobile networks are increasingly required to support operations at a large number of different bands. This is because the most common configuration is the inter-band non-contiguous CA, according to the latest 3GPP release. To fulfill the requirements of spectrum coverage, wideband systems have recently received a great deal of research interest.

As the most critical component in the RF chain, the power amplifier (PA) presents significant impacts on the systems. Research efforts have long been centered on the design of broadband PAs [1]–[10], since it allows great flexibility in transceiver designs.

These excellent demonstrations use either analytical [12]–[20] or numerical [21]–[23] method while extracting the parameters of the synthesized broadband impedance matching network (BIMN). Meanwhile, it is worthwhile pointing out that the implemented BIMNs are based on the low-pass ladder structure, almost without exception. This is because the low-pass ladder is one of the most practical topologies for broadband matching, and is commonly considered for simplicity in synthesis and physical construction.

Since the tabulated data in [20] offers a practical and efficient means to obtain the initial values of the ladder network, [1]–[7] make direct use of these tables to design the low-pass BIMN that is based on the real-to-real Chebyshev impedance transformer. In particular, [6] reports a modified network, namely the Elliptic low-pass BIMN, where the first shunt capacitance is replaced by the LC series resonance. The broadband PAs using the real frequency technique (RFT) have also been reported in [8]–[11]. Again, the constructed BIMNs are still based on the LC low-pass ladder structure,

because the derivations are performed under the condition of $f(p) = 1$, detailed elsewhere [23].

It is commonly accepted that the deviations of efficiency contours from the power contours complicate the design of broadband PAs. However, in fact, the phenomenon of opposite impedance rotation is one of the main technical challenges in broadband PA implementations. Specifically, the extracted optimum source ($Z_{S,OPT}$) and load impedance ($Z_{L,OPT}$) exhibit a counterclockwise shifting trend versus increasing frequency, whereas the impedance trajectory of the realizable passive matching networks rotate clockwise. To the best knowledge of the authors, it is Wu *et al.* [8] who report this design constraint for the first time. Similar observations are reported in [7], [9], and [24]–[26] as well.

This negative phenomenon constrains the realization of broadband PAs, but rarely has a research group endeavored to figure out an effective solution. Although multiple designers have expended substantial efforts to overcome such a problem by optimizing the reactive terminations at harmonic frequencies [2]–[7], [26]–[28], the impedance trajectories of the constructed BIMNs do not differ essentially from those in the preceding demonstrations, such as [1] and [8].

Objectively, the low-pass topology is proven to be an effective structure in extending the bandwidth. A key strength of the low-pass BIMN is the purely reactive terminations achieved at the harmonics [1]–[7]. No one would deny that harmonic termination of this type is more preferred in high efficiency mode of operations, such as Class J or continuous Class F/F^{-1}. But on the other hand, the main shortcoming of the synthesized low-pass BIMN is the inadequate BIR at the fundamentals. Considering the fact that the transistor depends more heavily on the fundamental termination, continuous investigation on the most adequate BIMN is fundamentally required.

Unlike the assumptions made in the literature, where the dominant reactive constraints (DRCs) of the PA are defined as the parasitic elements in the low-pass form, this paper makes a hypothesis that the DRCs of the transistor output can be represented by the RLC series resonant circuit (SRC). Since the band-pass networks are commonly considered to equalize the resonance of the load, design efforts are actually focused on the synthesis of the band-pass BIMNs, instead of elaborate optimization on the low-pass ladder structure.

The proposed band-pass BIMN can be constructed by modifying the equations outlined in [29], and this prototype was first reported by Matthaei in band-pass filter design. In [4], the third-degree band-pass BIMN is designed to equalize the series resonance at the transistor input. This paper further extends the prototype to fourth-degree, since adequate broadband impedance rotation (BIR) and improved compensation are expected with acceptable additional complexity.

Due to the negative phenomenon, namely opposite impedance rotation, the conventional BIMN in low-pass form cannot generate a BIR that is adequate for optimum broadband operation of the PA, and thus the main objective of this paper is to propose a reliable synthesis method so as to

yield the BIR which is curved in an optimized manner. The inadequacy will be outlined in Section III, and Section IV will primarily discuss the practical benefits of the band-pass BIMN. In Section V and VI, the systematic synthesis process and the measurements are presented, respectively.

II. PRELIMINARY DISCUSSION
A. PRACTICAL CHALLENGES IN BROADBAND PA IMPLEMENTATIONS

Fig. 1 describes the ''supply and demand'' problem in broadband PA designs. On the demand side, the $Z_{S,OPT}$ and $Z_{L,OPT}$, which are determined by varying the loading conditions [30], reveal the termination demands of the adopted transistor for the best performance of interest. Principally, the PA shall yield the promised performances in gain, efficiency, output power and linearity, as long as the transistor can see the prescribed $Z_{S,OPT}$ and $Z_{L,OPT}$. On the supply side, the $Z_{IN,IMN}$ and $Z_{IN,OMN}$ denote the impedance looking toward the input and output BIMN, respectively. Adequate Z_{IN_IMN} and Z_{IN_OMN} is a guarantee of good matching quality across the whole band of interest. Thus, from the viewpoint of impedance trajectory, the key challenge associated with broadband PAs is the design of optimum BIMN whose impedance trajectory is more consistent with the shifting trend of $Z_{S,OPT}$ and $Z_{L,OPT}$.
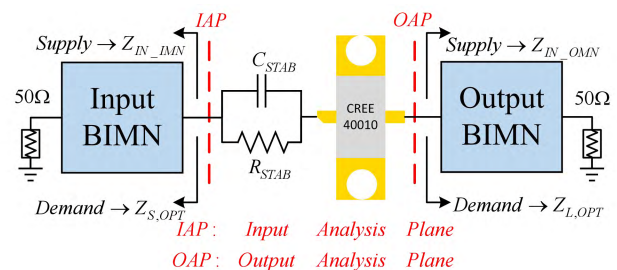

FIGURE 1. Block diagram in broadband PA designs. The BIMN can be considered as a lossless two-port impedance-transforming network terminated at one end in the standard resistance of 50 Ω. Suitable stabilization circuit (parallel R_{STAB} and C_{STAB}) is added in this design to ensure stable operation, then the analysis end should be moved backward at the input side.

B. BRIEF REVIEW OF BROADBAND MATCHING THEORY

The problem of broadband matching has been extensively covered, and several synthesis methods have been reported in the literature [12]–[23]. Generally, they can be divided into two major categories: analytical and numerical approach.

The analytical approach begins the derivations by assuming simple RL or RC load. optimum broadband network is required to equalize the reactive components over a wide bandwidth. Based on rigorous maths, Fano [12] has derived the theoretical limitations on the tolerance of mismatch and bandwidth. Matthaei [13], Bennett [14], Fielder [15] and Chen *et al.* [16], [17], extend Fano's work and report the synthesis methods for certain types of RLC loads. For instance, Chen et al. address a matching problem of practical interest,

where the load consists of an inductance in series with a parallel RC combination (one of the many possible extensions of Fano's work). Besides, Bennett and Fielder are devoted to the broadband matching of multi-degree LC ladder load. The RFT [21]–[23], a good representative of the numerical analysis, employs programmed iteration technique to achieve rapid convergence and thus offers an alternative in the extraction of the design parameters.

Particularly, it is worth noting that the matching networks in low-pass, high-pass and band-pass form can be synthesized in analytical approach, whereas the RFT only reports the design of low-pass network. The simplest form of $f(p)$ is employed, where $f(p)$ is a constant and is normalized at unity ($f(p) = 1$ corresponds to the LC low-pass ladder network [23]). This assumption dramatically simplifies the computation of the strictly Hurwitz polynomial of $g(p)$ using (1). For the $f(p)$ in more complex form, such as p^k, the synthesis method has not been reported in the literature.

$$g(p) \cdot g(-p) - h(p) \cdot h(-p) = f(p) \cdot f(-p) \qquad (1)$$

It is important to point out that broadband matching can be considered as a bandwidth extension theory, and it is the curved impedance trajectory that extends the bandwidth. Sun and Jansen [24] present qualitative vector analysis by evaluating the frequency-dependent parameter γ ($0° \leq \gamma \leq 180°$). In the scenario of narrowband matching, γ will be always greater than 90°. The impedance trajectories behave similarly to arcs with a coincidence only at the specified design frequency, and at other frequencies they rarely make an intersection again [see Fig. 5(a) in [24]]. Broadband matching occurs when the impedance trajectory is curved, which leads to decreased γ ($< 90°$), forming the BIR within the designated impedance region.

III. PHENOMENON OF OPPOSITE IMPEDANCE ROTATION AND THE RESULTING DESIGN CONSTRAINTS

The PA demonstrations reported in [7]–[9] and [24]–[26] confirm the practical constraint in broadband PA designs. Based on the preliminary design examples in [1] and [7], sub-section B illustrates the rotation profiles.

As will be shown in Section III-B, the impedance trajectories of the synthesized low-pass BIMNs can only exhibit a BIR within a fixed impedance region. Therefore, in principle, the low-pass BIMN is valid in broadband matching of the load that can be represented by a fixed impedance, but has decreased effectiveness in the use for broadband matching of the active devices, such as the PA, where the $Z_{S,OPT}$ and $Z_{L,OPT}$ are frequency dependent.

A. COUNTERCLOCKWISE IMPEDANCE MOVEMENT
Considering that the load pull techniques offer the ultimate characterizations of the large signal behavior [30], the simulated contours in Fig. 2 are employed to determine the most appropriate termination impedances so as to optimize the power added efficiency (PAE) and output power (P_{OUT}).
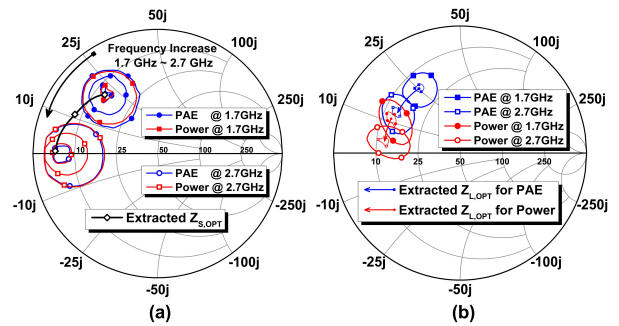

FIGURE 2. Simulated impedance contours of PAE and P_{OUT}. (a) Source pull contours, where $R_{STAB} = 50\ \Omega$, $C_{STAB} = 3.0$ pF. (b) Load pull contours.

The plots that are marked with small symbols depict the impedance regions that promise the best performance of interest. One can perceive a series of concentric circles in source pull simulations, whereas the output PAE contours deviate from those for POUT, indicating that compromises between efficiency and power is inevitable at the PA output.

It is obvious that the preferred loading conditions vary over frequency. Approximately, the extracted source pull and load pull contours are steadily moving down along the resistance circle as frequency increases, forming counterclockwise impedance movement.

B. CLOCKWISE IMPEDANCE ROTATION
Impedance matching issue can be analyzed by investigating the impedance trajectory on the Smith Chart, since it offers practical insights into the synthesized BIMNs. Fig. 3 illustrates the typical demonstrations of the low-pass BIMNs, and the numerical parameter values are listed in Fig. 3(b). Although it is reported that the RFT can achieve broadband matching by evaluating the gain bandwidth limit, there is no significant difference in the rotation of the impedance trajectory.
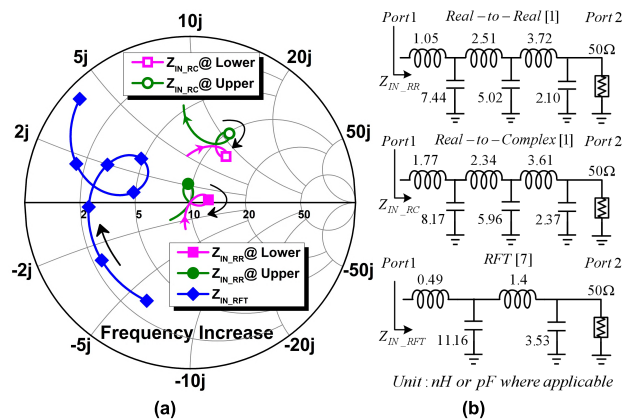

FIGURE 3. (a) Standard BIR of the low-pass BIMNs based on the Chebyshev impedance transformer [1] and the RFT [7]. The Smith Chart is normalized to 10 Ω. (b) Corresponding circuit schematic consisting of series inductance and shunt capacitance, and the impedance at port 2 is transformed to the standard 50 Ω.

Clearly, the impedance trajectories exhibit clockwise BIR over a wide bandwidth. Besides, it is obviously that the four-degree low-pass BIMN can yield only a single BIR, and the six-degree network generate two individual BIRs highlighted in magenta and green, respectively.

C. EXISTING DESIGN CONSTRAINTS OF THE LOW-PASS BIMNs

The low-pass BIMNs are commonly used not only in the early era of amplifier designs [31], [32], but also in the most recent PA implementations [1]–[11]. The reasons behind are twofold. In the first place, numerous researchers [12]–[22] have reported their excellent work on the synthesis procedures. In the second place, based on the standard distributed design method, the series inductance and shunt capacitance can be easily converted into the equivalent distributed circuits.

In the broadband PA demonstrations using the low-pass BIMNs, such as [1]–[11], one of the main design criteria is to yield the BIR roughly inside the intersections of the extracted contours over the whole band of interest while simultaneously achieve harmonic matching, attempting to further enhance the PAE. In [1]–[7], the broadband real impedance transformation is obtained from the tabulated data in [20], and then the reactive elements involved are manually tuned to reposition the BIR [see Z_{IN_RC} in Fig. 3]. Similar BIR can also be obtained via the RFT [see Z_{IN_RFT}].

From the perspective of the impedance trajectory, suboptimal broadband impedance transformation is expected when the low-pass BIMN is employed, and it is reasonable to point out the inadequacy. Recall the trajectory representations in Fig. 2, optimum broadband operation of the PA requires a load impedance with decreased imaginary component versus increasing frequency. However, as depicted by the locus of Z_{IN_RC} in Fig. 3(a), the imaginary part of the upper-half band BIR is larger than that of the BIR in the bottom position. It is obvious that the rotation of this type is completely contrary to the movement of the simulated contours.

Since the BIR of the classical low-pass network is commonly curved within a fixed impedance region, designers have no choice but to position the BIR at the impedance region where the $Z_{L,OPT}$ of the central frequencies locates. Therefore, it can be concluded that the low-pass BIMN can be employed to extend the bandwidth, but often at the sacrifice of the matching quality at the band-edge frequencies. More specifically, at the lower portion of the band, the BIR is close to the power contours, indicating that the transistor is expected to operate less efficiently, but can yield higher saturated output power (P_{SAT}). But on the other hand, despite the fact that the PA has increased potential for highly efficient operation at the uppermost frequency, it usually suffers from low P_{SAT}, and gain compression appears to become significant at relatively low power levels.

To make matters worse, the opposite impedance rotation accelerates the impedance mismatch, and the resulting mismatching would lead to the variations in gain, efficiency, power and linearity in many aspects. As depicted in Fig. 29 and 34 of [25], the measured PAE exhibits a significant drop at the band-edge frequencies. In fact, it has been becoming a default rule that designers have to tolerate performance variations or even degradations [8], [25] in broadband PA implementations. The wider the bandwidth, the more tolerances are expected.

After realizing the design constraints outlined above, several researchers attempt to overcome such a problem through extensive optimization of the low-pass BIMN. For instance, in [4] and [5], the authors choose to abandon the standard BIR to compensate the matching quality at the upper portion of the band. A modified low-pass network has also been reported in [6], namely Elliptic low-pass BIMN. In [9] and [10], a solution using the RFT has been presented. However, there is no significant breakthrough in adequate BIR for optimum broadband operation of the PA.

It's worth pointing out that the low-pass BIMN that is conventionally used in the literature is based on the Chebyshev real-to-real impedance transformer [20], which reveals that this prototype is ideal for the applications where frequency-invariant impedance is terminated on both sides. However, the key fact that distinguishes PA designs from conventional passive circuit design is that the optimum impedance of the PA is frequency dependent. It is unfair to ignore this frequency dependent nature, and no doubt, it is designers' obligation to compensate the frequency-variable response of the PA.

IV. PROPOSED BROADBAND MATCHING STRATEGY IN BAND-PASS STRUCTURE

In the classic analytical approach, such as Fano's optimum broadband matching theory, simple RL or RC load is used. But even if the topology of the load is considerably more complicated than that discussed by Fano, which is usually the case in practical PA designs, it is still possible to make a solid analysis on the DRCs under study. Then, analytical design approach can be developed in an analogous manner.

Investigation starts from the detailed evaluation of the equivalent circuit model of the GaN HEMT, attempting to make a hypothesis that the DRCs of the packaged transistor can be modeled more closely by the SRC. Then, further evaluation of the potential topologies for broadband matching has revealed the band-pass type network to be an appropriate structure. The qualitative analysis and quantitative simulations are introduced as supplementary supports to the conclusion made in this section.

A. ANALYSIS BASED ON EQUIVALENT CIRCUIT MODEL

Despite the fact that equivalent circuit approach cannot precisely characterize the nonlinearity exhibited by the PA, and load pull data shall prevail in case of any discrepancy [34], it is important to point out that the circuit analysis can provide reliable insight and solid guidance on the selection of the most appropriate topology.

Several researchers have reported their findings in transistor modeling [35]–[38]. In this paper, the valid equivalent circuit model reported in [35] has been employed. Similar circuit configuration has been used in the relevant literature [1]–[4], [6], [9]. The unilateral simplified circuit is shown in Fig. 4(a), assuming that the device is lossless. The elements enclosed by the dashed line represent the oversimplified equivalent circuit which is more adequate for the design using bare die transistor. In this case, the transistor should yield optimal performance, if the parasitic capacitances (series C_{GS} or shunt C_{DS}) can be equalized [32], [33].
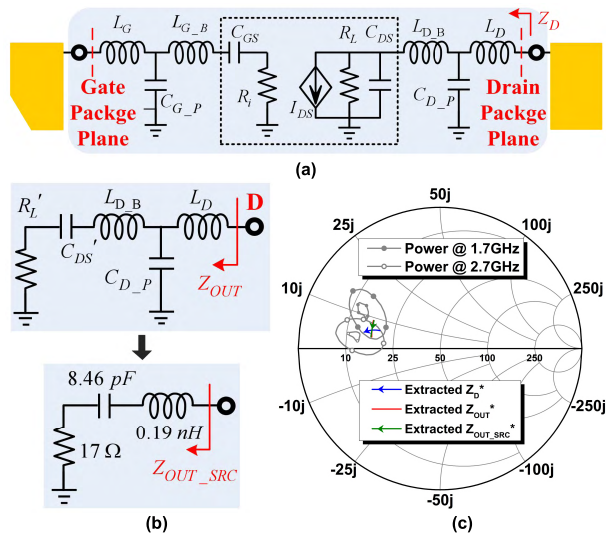

FIGURE 4. (a) Simplified schematic representation of the packaged GaN HEMT device. Empirically $R_L \approx 26\ \Omega$, $C_{DS} = 1.3$ pF. (b) Equivalent circuit after parallel-to-series conversion, where $R_L' = 21.34\ \Omega$, $C_{DS}' = 7.26$ pF, $C_{D\_P} = 1$ pF, and $L_{D\_B} = L_D = 0.3$ nH. (c) Conjugate of Z_D, Z_{OUT} and Z_{OUT_SRC} (frequency sweep range: 1.7-2.7 GHz).

In most cases, the packaged transistor is commonly used, where the intrinsic current source is masked by extrinsic and package parasitic elements. Cree does not release relevant details in their official documents. Fortunately, the application note from Nitronex [39] gives a good estimate of these parasitic elements, including L_G, L_D, L_{G_B}, L_{D_B}, L_{G_P}, and L_{D_P}.

In terms of the intrinsic parasitic components, the output resistance R_L, shunting the drain current source, represents the internal resistance. As discussed in classical load-line theory, the real part for a power match can be roughly calculated using the math by

$$R_L = (V_{DS} - V_{knee})^2 / 2P_{out} \qquad (2)$$

where $V_{DS} = 28$ V, $V_{knee} \approx 5$ V, $P_{out} = 10$ W for the adopted transistor. Given that C_{DS} is a weak function of bias voltage and frequency [36], [37], it is appropriate to assume $C_{DS} = 1.3$ pF (the typical value listed in the transistor datasheet). Although the nonlinear C_{DS} has been evaluated in [40], most research groups [36]–[38] usually treat C_{DS} as a bias-invariant element.

The discussion outlined below attempts to determine the DRCs of the PA and give a reasonable approximation on the fact that the load pull contours exhibit a steady movement along the resistance circles in the Smith Chart.

Using the parallel-to-series conversion defined in (3) and (4), the parallel combination of R_L and C_{DS} can be equivalently converted into a series network, as shown at the top of Fig. 4(b). Simply calculation gives the value of R_L' and C_{DS}'. Equation (3) indicates that R_L is transformed down by a factor of $1 + (Q_P)^2$, where Q_P is the quality factor of the network consisting of R_L and C_{DS}.

The low-pass L-section network (C_{D_P} in parallel with L_D) would transform R_L' to a smaller series value, and detailed discussion on this aspect can be found in standard microwave engineering books, such as [41]. Up to this point, the real part of Z_{OUT} has decreased from 21.34 Ω to about 17 Ω, which shows a good agreement with the load pull simulation, where the real part of $Z_{L,OPT}$ is around 15 Ω.

$$R_L' = \frac{R_L}{1 + (Q_P)^2} = \frac{R_L}{1 + (\omega R_L C_{DS})^2} \qquad (3)$$

$$C_{DS}' = \frac{1 + (\omega R_L C_{DS})^2}{(\omega R_L C_{DS})^2} C_{DS}$$

$$Z_{OUT} = \frac{R}{1 + (\omega R C_{D\_P})^2} + j[\omega L_D - \frac{\omega C_{D\_P}}{(\omega C_{D\_P})^2 + R^{-2}}], \qquad (4)$$

where

$$R = R_L' + j[\omega L_{D\_B} - (\omega C_{DS}')^{-1}] \qquad (5)$$

In principle, Z_{OUT} can be mathematically calculated using (5), but it would be extremely tedious to go through the computations over a wide frequency range. Herein, ADS 2011 from Keysight is used to simplify the computations involved.

Fig. 4(c) depicts the conjugate of the output impedance in the Z-Smith Chart as function of frequency. The plots in light gray represent the extracted P_{OUT} contours. Refer to the blue plot, the parasitic networks in the low-pass arrangement are not supposed to produce decreased imaginary part with increase in frequency. But on the other hand, the trajectory of Z_{OUT}^* exhibits a movement that is analogous to the shifting trend of the load pull contours, despite of the slight deviation. The reason for this deviation is complicated. One possible explanation is that nonlinearity dominates the transistor output, and the circuit analysis based on the linear S-parameter is inadequate for the precise characterization of the nonlinearity exhibited by the PA.

Note the series combination of 8.46 pF and 0.19 nH can approximately yield analogous frequency response of the circuit shown at the top of Fig. 4(b) [see the red and green plot in Fig. 4(c)]. Then it is valid to conclude that the DRCs at the transistor output can be represented by the simplified SRC. This fact is key in the hypothesis of broadband output matching using the band-pass structure, since the band-pass BIMN is the best candidate to equalize the series or shunt resonance. Meanwhile, it is reasonable to question whether

the low-pass ladder is the most appropriate structure in the problem of broadband matching of the transistor output.

B. METHODOLOGY USING BAND-PASS BIMNs
1) FEASIBILITY DISCUSSION
So far, little research work relating to the implementation of the band-pass BIMN in distributed form has been reported, but the feasibility in lumped form has been analytically addressed in [12].

Further investigations indicate that the band-pass matching networks can be used to match any of the loads in low-pass, high-pass or band-pass form. For instance, Bennett [14] points out that the *LC* low-pass or band-pass matching network should be designed to match the load in low-pass form. For the case of *LC* high-pass load, the high-pass or band-pass matching network should be used in principle. Similar conclusions have also been reported by Matthaei [see Fig. 2, 10 and 14 in [13]]. As for the load consisting of single reactive component, Chen and Kourounis [17] and Levy [18] have presented step by step procedures in absorbing the series *C* or shunt *C* into the synthesized band-pass BIMNs. Based on this synthesis method, a systematic approach to the implementation of the broadband PA has been reported in [33].

Therefore, regardless of how the BIMN could be constructed, the core is that the optimum BIMN must be designed to equalize the reactive constraints of the load. In other words, these reactive components or the DRCs shall be either tuned out or absorbed into the synthesized BIMN, leaving a pure real-to-real impedance transformation [12]–[19], [31]–[33].

2) PRACTICAL BENEFITS OF BAND-PASS BIMN
Fig. 5 illustrates the prototype and the impedance trajectory of the band-pass BIMN. The simulation is based on the examples presented in [19]. Unlike the hypothesis made in [19] and [33], where the single shunt capacitance is treated as the DRC, the reactive components under consideration in this case are the RLC SRC, which means the analysis should be performed at the plane AA' or BB'.

Fig. 5(a) depicts the circuit with symmetrical resonance, where the band of interest is centered at the resonance frequency of the resonant load. The impedance trajectory in this case exhibits real-axis symmetry. For the case of the unsymmetrical resonance shown in Fig. 5(b), it confirms the feasibility of repositioning the impedance trajectory [see Fig. 5(c)]. The slight deviation in the S-parameters reveals that adequate broadband impedance transformation is available for both unsymmetrical and symmetrical resonant load.

More importantly, one may notice that the impedance trajectory of the four-degree band-pass network has a number of unique benefits over that of the six-degree low-pass approach. One of the most significant is that the BIR of the lower-half band is in the top position, and the BIR of the upper-half band is in the bottom position. Compared with the impedance trajectory in Fig. 3(a), this unique rotation
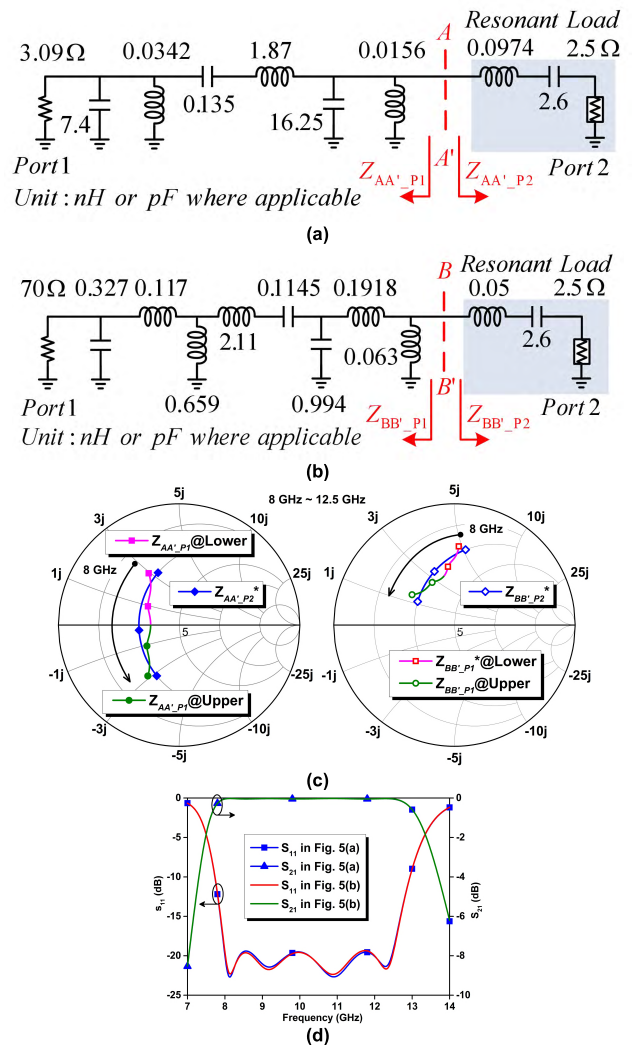

FIGURE 5. (a) Fourth-degree band-pass prototype before impedance transformation (duplicate of Fig. 6(b) in [19]). (b) Equivalent prototype after upward impedance transformation (duplicate of Fig. 7(a) in [19]). (c) Simulated impedance trajectories at the reference plane AA' and BB' (normalized to 5 Ω). (d) Simulated S-parameters.

property is expected to yield a good compensation method, which enables the impedance trajectory to be largely consistent with the movement of the load pull contours.

3) IMPLEMENTATION DIFFICULTIES
Although the band-pass type structure is a versatile topology, the band-pass network is not usually the top choice in practice. Part of the reason is that the number of the reactive elements involved should be at least doubled. Besides, implementation difficulties arise, since the approximation to the resonance and the series capacitance is more complicated than the implementation of the series inductance and shunt capacitance in low-pass scheme.

The design consideration relating to this aspect was addressed by Saad *et al.* [33], as shown in Fig. 6, where a surface-mount capacitor is used to approach the series
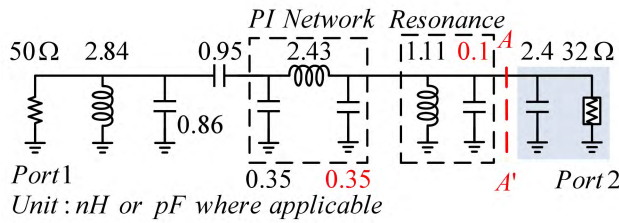
FIGURE 6. Broadband four-degree Band-pass matching network reported in [33]. Since the single shunt capacitance is treated as the DRC, the analysis plane is located at plane AA'.

capacitance of 0.95 pF. This lumped capacitor has a dual role of impedance matching and dc block. However, the hybrid of lumped and distributed elements in the interior of the BIMN is less preferred due to the lack of accuracy. In addition, the shunt capacitor of 2.85 pF is split to give the desired capacitance (C_{OUT}) value of 2.4 pF, with the remainder being divided into two shunt capacitors of 0.1 and 0.35 pF. Then two lumped-to-distributed equivalences are individually introduced to approximate the lumped PI network and the parallel resonance [33], [41]. It is believed that the transformations of this type may become a major source of inaccuracy.

4) PROPOSED BAND-PASS BIMN FOR SRC LOAD

Again, the practical challenge now confronting PA designers is the physical implementation of the band-pass BIMN in distributed form. Matthaei [29] addresses a practical method for the synthesis of wideband band-pass filters in the form of quarter-wavelength stubs and connecting lines, and explicit design equations are given.

In this case, the lumped circuit elements are not individually replaced by the corresponding distributed components. In fact, the characteristic admittances of the stubs and the connecting lines are theoretically calculated as a whole to equalize the resonant response of the load. It is recognized that this synthesis method ensures high precision in electromagnetic simulation and therefore is used to construct the proposed band-pass BIMN. Besides, the parameter d is used to give the appropriate impedance level of the stubs and connecting lines, which offers great flexibility in theoretical calculation and is particularly useful in hardware implementation.

V. IMPLEMENTATION OF THE PROPOSED BAND-PASS BIMN

A. PROCEDURE FOR DERIVING THE EQUATIONS

It is commonly accepted that the increase in n, where n denotes the number of reactive elements in the corresponding low-pass prototype, will not yield improvements linearly [12], [13], [18], [19]. Although less improvement in matching quality is expected, this paper extends the derivations to the case of $n = 4$, because it is possible to obtain two individual BIRs at the lower- and upper-half band of interest [19].

The proposed band-pass BIMN can be readily designed by a modified use of the equations presented in [29].

Since, the synthesis procedure for $n = 3$ has been addressed in [4], only the key differences will be outlined herein.

With regard to the computation of the normalized g elements (g_k) in the low-pass Chebyshev prototype, it is needed to clarify two aspects. The first one is that the three-degree polynomial that is used to compute sinh a and sinh b is different, as shown in (6):

$$16(xy)^3 + 8(xy)^2 + (2 + 8\delta^2)(xy) - (1 + 2\delta^2) = 0 \quad (6)$$

where $x = $ sinh a, $y = $ sinh b, $\delta = (Q\omega)^{-1}$, Q is the quality factor of the load to be matched in the normalized prototype, ω is the fractional bandwidth. The next one is the equation for the parameter D, as shown in (7).

$$D = \frac{\sinh a}{\delta \sin(\pi/8)} - 1 \quad (7)$$

For band-pass filter of the form shown in Fig. 7(a), [29] gives the explicit equations for each interior section. The modified prototype used to derivate the equations for the proposed $n = 4$ band-pass BIMN is shown in Fig. 7(b), with the right end connected to an extra J-invertor. One of main differences is that the impedance transformation ratio r ($r > 1$) is introduced in this case, indicating that upward
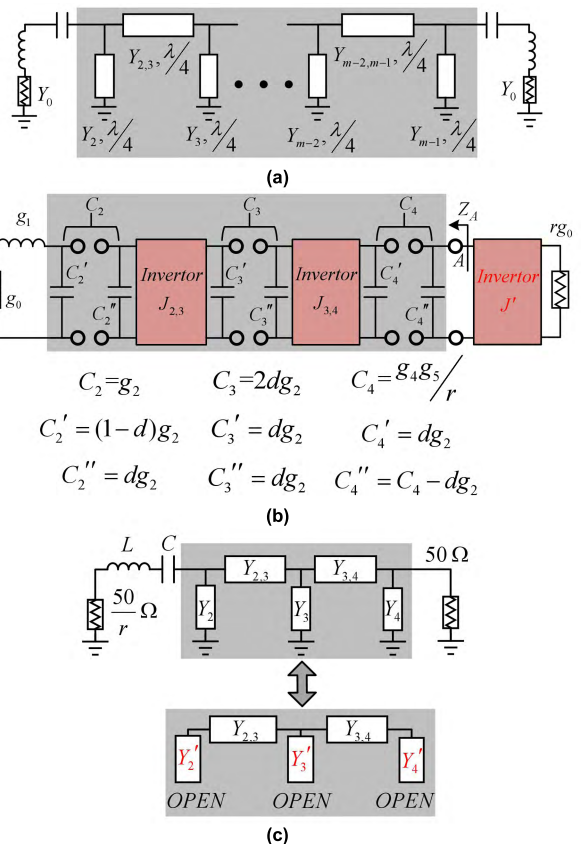

FIGURE 7. (a) Diagram of the band-pass filter with λ/4 stubs and λ/4 connecting lines. (b) Modified prototype for deriving the equations for he proposed n = 4 band-pass BIMN. (c) Diagram of the proposed n = 4 band-pass BIMNs.

impedance transformation is required, whereas filters are synthesized for equal termination resistance.

Equ. (8) gives the normalized admittance of the $\lambda/4$ connecting line.

$$\frac{J_{2,3}}{Y_0} = \frac{1}{g_0}\sqrt{\frac{C_2 C_3}{g_2 g_3}}, \tag{8a}$$

$$\frac{J_{3,4}}{Y_0} = \frac{1}{g_0}\sqrt{\frac{C_3 C_4}{g_3 g_4}}. \tag{8b}$$

As was done in [29], C_3 is twice the value of $C_\alpha = dg_2$. Besides, the admittance of the additional J-invertor should satisfy

$$\frac{J'}{Y_0} = \frac{1}{g_0}\sqrt{\frac{C_4 r g_0}{g_4 g_5}}. \tag{9}$$

Considering that upward impedance transformation is achieved at node A, let $J' = 1$ in (9), and solve for C_4.

Up to this point, the closed-form design equations have been derived. The value for Y_2 and Y_3 can be calculated using (10a) and (10b), respectively. Substituting C_4'', $M_{3,4}$ and $J_{3,4}$ for C_2', $M_{2,3}$ and $J_{2,3}$, respectively, gives the equation for the third shunt stub Y_4. In consideration of lab tuning and board fabrication, the short-circuited $\lambda/4$ stubs are replaced by the equivalent open-circuited $\lambda/2$ stubs [see Fig. 7(c)], which means the calculated Y_k should be multiplied by a factor of K.

$$Y_2 = \frac{Y_0 \omega_1'(1-d)g_2}{g_0}\tan\theta + Y_0\left(M_{2,3} - \frac{J_{2,3}}{Y_0}\right) \tag{10a}$$

$$Y_3 = Y_0\left(M_{2,3} - \frac{J_{2,3}}{Y_0} + M_{3,4} - \frac{J_{3,4}}{Y_0}\right) \tag{10b}$$

$$Y_4 = \frac{Y_0 \omega_1' C_4''}{g_0}\tan\theta + Y_0\left(M_{3,4} - \frac{J_{3,4}}{Y_0}\right) \tag{10c}$$

$$M_{k,k+1} = \sqrt{\left(\frac{J_{k,k+1}}{Y_0}\right)^2 + \left(\frac{\omega_1' C_\alpha \tan\theta}{2g_0}\right)^2} \tag{10d}$$

$$\theta = \frac{\pi}{2}\left(1 - \frac{\omega}{2}\right) \tag{10e}$$

$$K = \frac{\tan^2\theta - 1}{2\tan^2\theta}. \tag{10f}$$

B. BAND-PASS BIMN IMPLEMENTATION

The proposed synthesis procedure comprises two main steps. It begins with the determination of the appropriate δ and ω from the given SRC, followed by the computations using (8) to (10).

The synthesis of the input BIMN will be first described, and then, the remainder of this sub-section will particularly highlight the design considerations of the output BIMN. Table 1 is a tabulation of the parameters for the case of symmetrical resonance. Since the imaginary component of the extracted $Z_{S,OPT}$ and $Z_{L,OPT}$ is unsymmetrical about the central frequency, empirical design technique is outlined to reposition the BIRs.

TABLE 1. Computed initial parameters for the proposed band-pass BIMNs.

Parameters	Input	Output	Parameters	Input	Output
r	10	3.33	g_5	1.85	1.08
ω	0.5	0.7	$Y_2{}^a$	0.378	0.0985
δ	0.48	1.5	Y_3	0.0655	0.0222
d	0.15	0.25	Y_4	0.0147	2.61×10^{-4}
g_0	1	1	$Y_{2,3}$	0.0646	0.0467
g_1	2.1	0.67	$Y_{3,4}$	0.0278	0.0266
g_2	0.86	1.10	$Y_2'{}^b$	0.157	0.0307
g_3	2.47	1.12	Y_3'	0.0271	0.00693
g_4	0.41	0.48	Y_4'	6.1×10^{-3}	8.14×10^{-5}

^{a}: De-normalized admittance in theoretical calculations (the unit is S).
^{b}: De-normalized admittance of the open-circuited $\lambda/2$ shunt stubs.

1) DESIGN PROCEDURES FOR INPUT BIMN

Step 1: Compute the parameter ω and δ. Since the frequency range is from 1.7 to 2.7 GHz, the value of ω is 0.455. The computations outlined in Table 1 use 0.5 to ensure good optimization margin. Recall the source pull contours in Fig. 2(a), the imaginary part of $Z_{S,OPT}$ varies from $+j21$ to $+j1$, approximately, indicating that the variation of $j20$ is required. As shown in the de-normalized band-pass prototype in Fig. 8(a), the SRC of 3.3 pF and 1.67 nH is determined, because it can yield the symmetric resonance from $+j10$ to $-j10$ over the frequency range of interest. Having values for Q and ω, the parameter δ can be calculated.
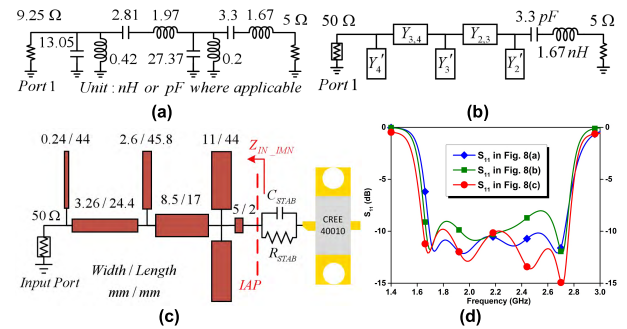

FIGURE 8. (a) Circuit schematic after frequency and impedance scaling (a) Band-pass network with symmetrical resonance. (b) Band-pass network with upward impedance transformation of 9.25 Ω to the standard 50 Ω. (c) Optimized band-pass BIMN ($\varepsilon_{r,eff} = 2.55$, lamina thickness is 30 mil). (d) Simulated S-parameters.

Step 2: Construct the circuit in lumped prototype with the desired passband characteristic from the computations of g_k [see Fig. 8(a)].

Step 3: Calculate the admittance Y_k and Y_{k+1} by use of the modified design equations. The lump-based circuit is directly converted into the distributed band-pass network with appropriate upward impedance transformation [see Fig. 8(b)]. Then, replace the short-circuited $\lambda/4$ stubs with the open-circuited $\lambda/2$ stubs.

Step 4: Reposition the impedance trajectory by adding a short length of pad [see Fig. 8(c)]. Since the reactance associated with the pad is positive inductance, the impedance trajectory of Z_{IN_IMN} will move up towards the upper

half plane. The dimensions of the pad can be determined empirically.

Fig. 8(c) depicts the physical dimensions of the proposed input BIMN. Balanced structure is used to give more practical dimensions of the first shunt stub. Since the calculated Y_4' is extremely small, the width of the third stub is set to 0.2 mm initially for practical reasons.

The simulated S_{11} in Fig. 8(d) confirms the matching quality of the circuits in Fig. 8(a) to (c), and Chebyshev equal-ripple response is achieved. The red plot reveal that the decreased impedance of the third stub has limited impacts, and the negative effects relating to this have been largely removed in layout optimization.

2) PARTICULAR CONSIDERATIONS FOR OUTPUT BIMN

The transistor input usually exhibits little nonlinearity, and compromise between efficiency and power is rarely needed at all [see Fig. 2]. In the case of input matching design, precise broadband impedance matching can be obtained as long as the DRCs of the transistor input can be equalized properly. While on the other hand, the transistor output is highly nonlinear. The impedance seen by the transistor output dominantly determines the efficiency and power over frequency. Therefore, special efforts are centered on obtaining the adequate BIR as part of a compensation to the negative phenomenon of opposite impedance rotation, rather than just equalizing the series resonance.

Under such a design criterion, appropriate design values for ω and δ are carefully determined. Again, the synthesis procedure begins by specifying $\omega = 0.7$, where large value of ω is chose to ensure sufficient margin for optimization. For the band-pass prototype with symmetrical resonance, the SRC of 1.04 nH and 5.3 pF is selected, giving a δ of about 1.5.

Following similar procedures, the output BIMN can be constructed. The simulated S_{22} for the prototypes in Fig. 9(a) and (b) are plotted in dB form in Fig. 9(c). The blue line reveals that the circuit in Fig. 9(a) supports much wider bandwidth, and as expected, good passband characteristic has been achieved from 1.4 GHz to 3 GHz.

One may notice that the matching quality of the circuit shown in Fig. 9(b) is worse than that of Fig. 9(a). The eason behind is that the nonlinear model from Cree is driven under small signal excitation. The large signal S_{22} extracted from harmonic balance simulation shows an overall improvements over the passband.

The red plot in Fig. 9(d) represents the impedance presented to the transistor drain flange, and the Smith Chart is normalized to 30 Ω to obtain the good resolution of the trajectory pattern. As expected, the $n = 4$ band-pass BIMN can yield two individual BIRs, depicting the impedance rotation of the lower- and upper-half passband, respectively. Although the band-pass BIMN exhibits counterclockwise impedance rotation, this particular BIR is curved in an optimized way, compared to that of the low-pass BIMN. Since the extracted $Z_{L,OPT}$ at high frequencies has decreased
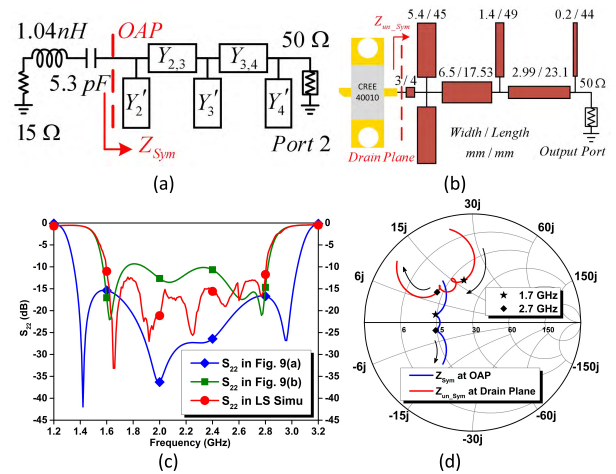

FIGURE 9. (a) Band-pass BIMN after upward impedance transformation. (b) Optimized band-pass BIMN after trajectory repositioning. (c) Simulated S_{22}. (d) Impedance trajectories of the band-pass BIMN at the fundamentals.

imaginary component, the BIR of this type reveals the good balance between PAE and P_{OUT} throughout the band of interest. In this case, the design constraints outlined in Section III can be largely compensated by the proposed BIMN in band-pass structure.

3) FLAWS IN HARMONIC TERMINATION

Harmonic impedance optimization is the core in high efficiency mode of operations. Theoretically, the definitions of the terminating loads at harmonics are different in Class E, Class F/F^{-1}, Class J and continuous Class F/F^{-1}. For example, Class J and F/F^{-1} operations assume purely reactive terminations or ideal open and short-circuit for harmonics, respectively. However, for the implementations of practical broadband PA, these idealistic assumptions would become an unrealistic expectation.

Unlike the evaluation method used in [2]–[7] and [33], namely harmonic phase simulation, an alternative design space has been introduced to enables precise harmonic characterizations. In this case, harmonic simulations with impedance sweep over the whole Smith Chart are performed, attempting to extract the optimum harmonic impedance region at each individual frequency. Fig. 10 shows the harmonic load pull simulations at 1.8, 2.2 and 2.6 GHz. The shaded area highlights the preferred termination demands at harmonic frequencies.

The plots in Fig. 11 depict the impedance trajectory of the proposed band-pass BIMN at the second and third harmonic frequencies. The arrow head indicates the direction of frequency increase. Clearly, a portion of the trajectory departs from the shaded impedance region, which reveals the risks of performance degradation in efficiency and power, such as 2.1–2.4 GHz. Fortunately, at most of the in-band frequencies, the harmonic impedance presented to the transistor drain lead is located within the shaded area, indicting a guarantee of high performances (depicted in blue in Fig. 11).
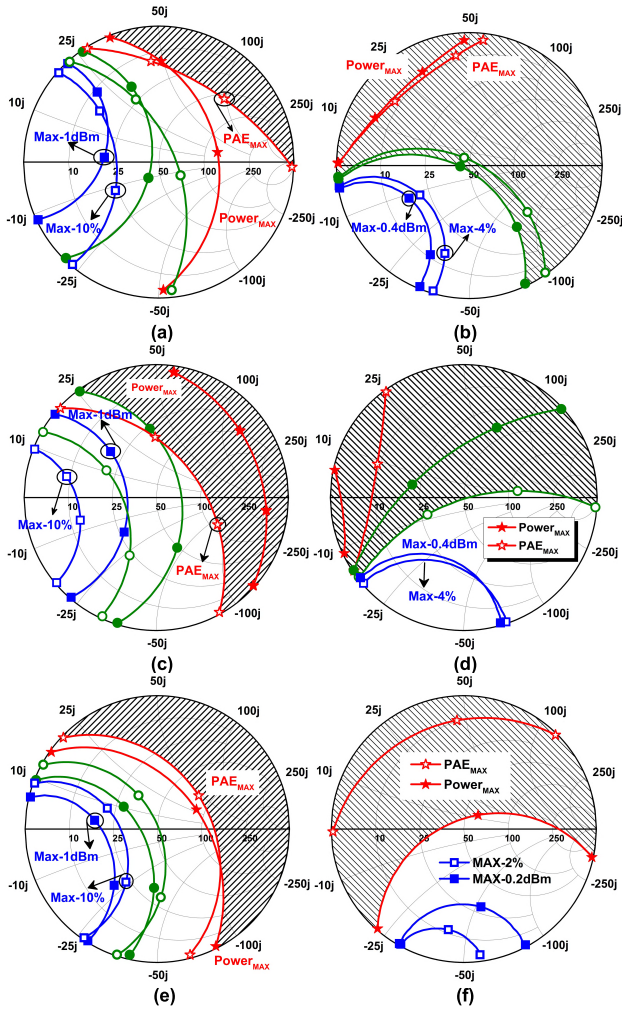
FIGURE 10. Harmonic load-pull simulation (a) Second harmonic at 1.8 GHz, $Z_{L,OPT} = (15 + j * 15) \, \Omega$. (b) Third harmonic at 1.8 GHz, and empirically $Z_{2nd} = (0 + j * 50) \, \Omega$. (c) Second harmonic at 2.2 GHz, $Z_{L,OPT} = (15 + j * 12) \, \Omega$. (d) Third harmonic at 2.2 GHz, and empirically $Z_{2nd} = (0 + j * 50) \, \Omega$. (e) Second harmonic at 2.6 GHz, $Z_{L,OPT} = (14 + j * 10) \, \Omega$. (f) Third harmonic at 2.6 GHz, and empirically $Z_{2nd} = (0 + j * 50) \, \Omega$.
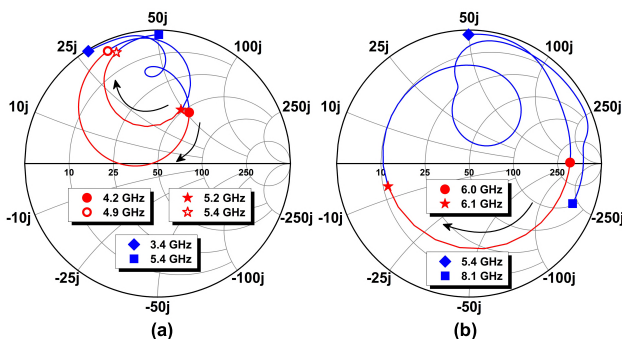

FIGURE 11. Impedance trajectory at (a) Second and (b) Third harmonic.

Frankly speaking, the simulation outlined above has exposed the flaw of the proposed BIMN in harmonic termination. According to the latest waveform engineering theory,

this flaw may degrade the PAE and P$_{OUT}$ to some degree. In fact, this drawback is largely due to the employment of the quarter wavelength connecting lines as well as the open circuited stubs. Since the transmission line is periodic with respect to the electrical length, long line sections imply the increased amount of the transmission bands at high frequencies. Thus, despite iterative optimization of the geometry of the proposed prototype, this standard band-pass BIMN can not yield efficient harmonic tuning.

In-depth investigations based on the modified band-pass structure have been developed to enhance the harmonic manipulation. The synthesis method relating to this design space will be included in the subsequent research work, where the objective is to achieve infinite attenuation at harmonic bands, enabling the harmonic terminations that is analogous to Class J or continuous Class F/F^{-1} operations [4], [26], [27].

VI. PA ASSEMBLY AND EXPERIMENTAL MEASUREMENTS

The proposed broadband PA is implemented on the Taconic TLX-8 substrate (30 mil thickness and $\varepsilon_r = 2.55$). The circuit diagram and top view of the PA implementation are shown in Fig. 12. Two surface-mount capacitors (15-pF) are connected at both ends as dc blocks, and the compact broadband bias chock is employed as the dc feed and RF isolation (4310LC from Coilcraft). In addition, the resistor R$_G$ is added to stabilize the transistor.
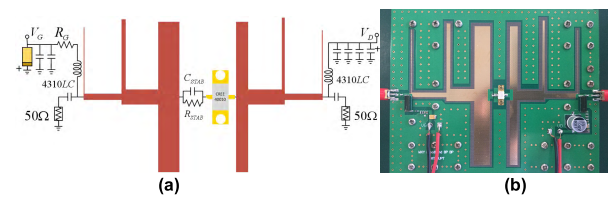

FIGURE 12. Layout diagram and photograph of the proposed PA.

The measurements and the simulation results in Fig. 13 verify the effectiveness of the proposed BIMNs. The proposed PA yields input and output return loss of about 13 dB minimum within the band of interest. Besides, the PA exhibits small gain fluctuations at the in-band frequencies, and the
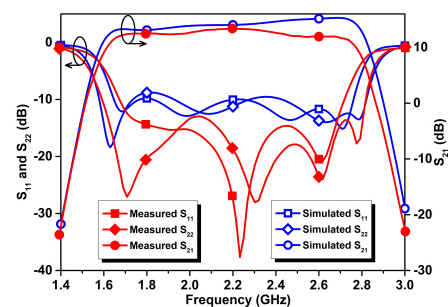

FIGURE 13. Simulated and measured S-parameters. The transistor is biased at the drain voltage and quiescent current of 28V and 60 mA.

gain that is available at the out-of-band frequencies decreases significantly. It can be concluded that the S-parameters give a clear illustration of where gain fades as a consequence of impedance mismatch. In this demonstration, we do not selectively mismatch the input of the transistor to flat the gain variations. Unexpectedly, however, the measured S_{21} shows an overall decline of about 2-3 dB in the upper portion of the band.

Large-signal measurements are carried out using the single-tone continuous wave (CW) signal from 1.7 to 2.7 GHz with 0.1 GHz step. The CW signals are pre-amplified by ZHL-16W-43-S+, the wideband Class-A PA from Mini-Circuits.

The transducer power gain and PAE versus P_{OUT} are plotted in Fig. 14. It can be seen that the measured PAE is greater than 60 % at the 3 dB compression point. In practice, the GaN HEMT amplifiers are rarely driven into the status with more than 3 dB drop in gain, because measured PAE and P_{OUT} would decrease rapidly, and severe nonlinearity is technically impossible to remove. Evidently, the matching quality across the second half of the band is not as good as expected. The gain tends to vary more widely than the measurements of the lower-half band, and the measured PAE rarely exceeds 60%. In particular, worst performance has been measured at 2.5 GHz, where the transistor becomes incapable of producing the rated output power ($P_{SAT} > 10$ W), but thereafter the P_{SAT} is gradually increasing back to normal levels. It is believed that the performance degradation at the upper-half band results from inadequate harmonic termination, as briefly outlined in Fig. 11.
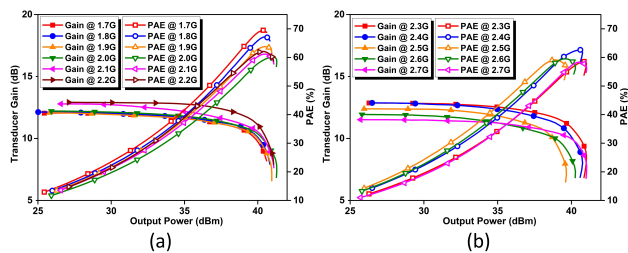

FIGURE 14. Measured gain and PAE in CW signal power sweeping.

Since PAs are often designed to increase efficiency, the transistors are currently exhibiting more and more nonlinear behavior. Digital predistortion (DPD) technique is introduced to explore the capability for linearization. Since crest factor reduction algorithm is not employed, the measured peak-to-average power ratio (PAPR) of the modulated signal determines the required power back-off in hardware test. As depicted in Fig. 15(a), the measured adjacent channel power ratio (ACPR) has been decreased to about −55 dBc at 6.5 dB power back-off. The average efficiency is about 39% PAE at 34 dBm output power. Similar test is performed when the proposed PA is driven by the 10-MHz WCDMA signal (about 7 dB PAPR). In this case, the DPD technique lowers the ACPR to about −50 dBc.
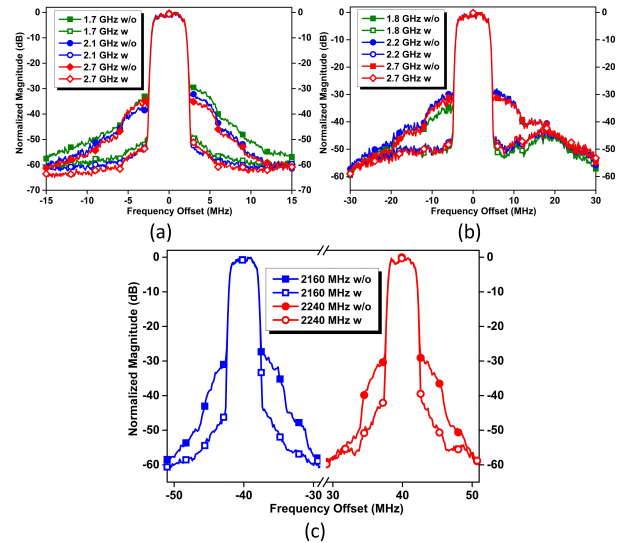

FIGURE 15. Measured spectra with and without DPD. (a) 5-MHz WCDMA signals. (b) 10-MHz WCDMA signals. (c) Concurrent dual-band excitation using 5-MHz WCDMA signals.

TABLE 2. Comparison of recent broadband PA implementations.

Ref.	MA [a]	Bandwidth (GHz)	FB [b] (%)	Gain ± GF [c] (dB)	Eff. [d] (%)
[1]	LP/LP	1-2	67	11.5±1.5	55-83 P [e]
[2]	LP/LP	1.3-3.3	87	15±2.5	58-80 P
[3]	LP/LP	1.3-3.3	87	16.5±1.5	58-78 P [f]
[4]	BP/LP	2-3	40	12±0.5	58-72 P
[5]	LP/LP	2-3.5	54	14±2	64-76 D
[6]	LP/LP	1.4-2.5	56	16±1	68-82 D
[7]	BP [g]/LP	1.8-2.7	40	Appx. 10	50-62 P
[8]	RFT LP	1.9-2.9	41	11.3±1.3	45-65 D
[9]	RFT LP	1.45-2.45	50	10.5±2.5	70-81 D
[10]	RFT LP	0.9-3	107	16±2	55-80 P
[11]	RFT LP	2.15-2.65	20	13.3±1.7	60-69 P
[25]	LP/LP	1.8-2.6	36	12.5±1.5	57-70 P
		1.2-2	50	Appx. 10	54-66 P
[26]	N/A [h]	0.5-0.9	57	18±1	75-84 P
[27]	N/A	0.55-0.95	53	17±1	70-77 P
This work	BP/BP	1.7-2.7	46	12.5±0.5	60-70 P

[a] MA: matching algorithm, LP and BP denote low-pass and band-pass, N/A denote not applicable.
[b] FB: fractional bandwidth.
[c] GF: gain flatness.
[d] Suffix P means PAE; suffix D means drain efficiency.
[e,f] Drain voltage is optimized for efficiency in CW test (not 28V).
[g] It seems like that the topology of the input BIMN is based on the Quasi-BP.
[h] Few details relating to the network synthesis method were reported.

Also noted that undesired memory effects have been observed at 1.7 and 1.8 GHz while evaluating the raw output signals. This negative phenomenon has been removed after DPD, since the upper and lower ACPR are of similar magnitude. Fig. 15(c) shows the concurrent measurement and linearization using two WCDMA signals with a frequency spacing of 80-MHz. The spectrum at 7 dB power back-off indicates that an ACPR of −50 dBc and −47 dBc has been measured when using the 2-D polynomial DPD algorithm.

Table 2 lists a summary of the main specifications of the most recent state-of-art broadband PAs. Some figures are obtained via the method of deduction or chart reading, since the complete assessment on PAE and gain versus P_{OUT} is not reported.

VII. CONCLUSION

The fundamental limitation in broadband PA designs is that passive matching networks can only produce positive phase dispersion, leading the impedance trajectory to rotate clockwise, whereas the extracted $Z_{S,OPT}$ and $Z_{L,OPT}$ usually exhibits counterclockwise movement versus frequency. This basic fact introduces additional restrictions in matching the transistor for optimum wideband operation.

Besides, the drawback of the conventional low-pass BIMN is that the BIR rotates in a very compact impedance region, which reveals that inadequate impedance transformation inevitably happens when frequency approaches the band-edges. The constraints resulting from inadequate BIR has been outlined in this paper

The main objective of this paper is to compensate the frequency-dependent behavior of the PA using the band-pass BIMN, and systematic methodology is presented. The core is that the DRCs of the package transistor are extracted, and load pull results are introduced as supplementary supports to the conclusions made herein. Then appropriate topology is determined accordingly, because the band-pass network is the most appropriate candidate to equalize the resonance of the load.

The proposed band-pass BIMN can satisfy the dual requirement of matching the DRCs of the PA over a wide bandwidth and offering adequate BIR that largely overlaps with the designated impedance region. Thus, good balance in terms of the matching quality over the whole band of interest can be obtained, and it is reasonable to believe that the band-pass BIMN shall be a realistic alternative to the low-pass solution.

Frankly speaking, design efforts involved in this paper have been focused on the compensation of adequate BIR at the fundamental frequencies, and it is unexpected that this standard band-pass BIMN is lack of strong impedance manipulation at harmonics. The next stage of research should focus on the modified band-pass structure so as to yield the harmonic terminations that is analogous to Class J or continuous Class F/F^{-1} operations.

REFERENCES

[1] K. Chen and D. Peroulis, "Design of highly efficient broadband Class-E power amplifier using synthesized low-pass matching networks," *IEEE Trans. Microw. Theory Techn.*, vol. 59, no. 12, pp. 3162–3173, Dec. 2011.

[2] K. Chen and D. Peroulis, "Design of broadband high-efficiency power amplifier using in-band Class-F^{-}1/F mode-transferring technique," in *IEEE MTT-S Int. Microw. Symp. Dig.*, Montreal, QC, Canada, Jun. 2012, pp. 1–3.

[3] K. Chen and D. Peroulis, "Design of broadband highly efficient harmonic-tuned power amplifier using in-band continuous Class-F^{-1}/F mode transferring," *IEEE Trans. Microw. Theory Techn.*, vol. 60, no. 12, pp. 4107–4116, Dec. 2012.

[4] X. Meng, C. Yu, Y. Liu, and Y. Wu, "Design approach for implementation of Class-J broadband power amplifiers using synthesized band-pass and low-pass matching topology," *IEEE Trans. Microw. Theory Techn.*, vol. 65, no. 12, pp. 4984–4996, Dec. 2017.

[5] J. Xia, X.-W. Zhu, and L. Zhang, "A linearized 2–3.5 GHz highly efficient harmonic-tuned power amplifier exploiting stepped-impedance filtering matching network," *IEEE Microw. Wireless Compon. Lett.*, vol. 24, no. 9, pp. 602–604, Sep. 2014.

[6] M. Yang, J. Xia, Y. Guo, and A. Zhu, "Highly efficient broadband continuous inverse Class-F power amplifier design using modified elliptic low-pass filtering matching network," *IEEE Trans. Microw. Theory Techn.*, vol. 64, no. 5, pp. 1515–1525, May 2016.

[7] T. Sharma, P. Aflaki, M. Helaoui, and F. M. Ghannouchi, "Broadband GaN Class-E power amplifier for load modulated delta sigma and 5G transmitter applications," *IEEE Access*, vol. 6, pp. 4709–4719, 2018.

[8] D. Y.-T. Wu, F. Mkadem, and S. Boumaiza, "Design of a broadband and highly efficient 45 W GaN power amplifier via simplified real frequency technique," in *IEEE MTT-S Int. Microw. Symp. Dig.*, Jun. 2010, pp. 1090–1093.

[9] N. Tuffy, L. Guan, A. Zhu, and T. J. Brazil, "A simplified broadband design methodology for linearized high-efficiency continuous Class-F power amplifiers," *IEEE Trans. Microw. Theory Techn.*, vol. 60, no. 6, pp. 1952–1963, Jun. 2012.

[10] Z. Dai, S. He, F. You, J. Peng, P. Chen, and L. Dong, "A new distributed parameter broadband matching method for power amplifier via real frequency technique," *IEEE Trans. Microw. Theory Techn.*, vol. 63, no. 2, pp. 449–458, Feb. 2015.

[11] N. Tuffy, A. Zhu, and T. J. Brazil, "Novel realisation of a broadband high-efficiency continuous Class-F power amplifier," in *Proc. IEEE Eur. Microw. Conf.*, Oct. 2011, pp. 120–123.

[12] R. M. Fano, "Theoretical limitations on the broadband matching of arbitrary impedances," *J. Franklin Inst.*, vol. 249, pp. 57–84, Jan. 150.

[13] G. Matthaei, "Synthesis of Tchebycheff impedance-matching networks, filters, and interstages," *IRE Trans. Circuit Theory*, vol. 3, no. 3, pp. 163–172, Sep. 1956.

[14] B. Bennett, "Broad-band impedance matching of ladder loads," *IEEE Trans. Circuits Syst.*, vol. 32, no. 12, pp. 1201–1208, Dec. 1985.

[15] D. Fielder, "Broad-band matching between load and source systems," *IRE Trans. Circuit Theory*, vol. 8, no. 2, pp. 138–153, Jun. 1961.

[16] W.-K. Chen, "Explicit formulas for the synthesis of optimum broad-band impedance-matching networks," *IEEE Trans. Circuits Syst.*, vol. CAS-24, no. 4, pp. 157–169, Apr. 1977.

[17] W.-K. Chen and K. Kourounis, "Explicit formulas for the synthesis of optimum broad-band impedance-matching networks II," *IEEE Trans. Circuits Syst.*, vol. CAS-25, no. 8, pp. 609–620, Aug. 1978.

[18] R. Levy, "Explicit formulas for Chebyshev impedance-matching networks, filters and interstages," *Proc. IEEE*, vol. 111, no. 6, pp. 1099–1106, Jun. 1964.

[19] D. E. Dawson, "Closed-form solutions for the design of optimum matching networks," *IEEE Trans. Microw. Theory Techn.*, vol. 57, no. 1, pp. 121–129, Jan. 2009.

[20] G. L. Matthaei, "Tables of Chebyshev impedance-transformation networks of low-pass filter form," *Proc. IEEE*, vol. 52, no. 8, pp. 939–963, Aug. 1964.

[21] H. J. Carlin, "A new approach to gain-bandwidth problems," *IEEE Trans. Circuits Syst.*, vol. CAS-24, no. 4, pp. 170–175, Apr. 1977.

[22] H. J. Carlin and J. Komiak, "A new method of broad-band equalization applied to microwave amplifiers," *IEEE Trans. Microw. Theory Techn.*, vol. 27, no. 2, pp. 93–99, Feb. 1979.

[23] B. S. Yarman, *Design of Ultra Wideband Antenna Matching Networks via Simplified Real Frequency Technique*. New York, NY, USA: Springer, 2008.

[24] G. Sun and R. H. Jansen, "Broadband Doherty power amplifier via real frequency technique," *IEEE Trans. Microw. Theory Techn.*, vol. 60, no. 1, pp. 99–111, Jan. 2012.

[25] W. Demenitroux, C. Maziere, E. Gatard, S. Dellier, M. Campovecchio, and R. Quere, "Multiharmonic volterra model dedicated to the design of wideband and highly efficient GaN power amplifiers," *IEEE Trans. Microw. Theory Techn.*, vol. 60, no. 6, pp. 1817–1828, Jun. 2012.

[26] T. Sharma, R. Darraji, and F. Ghannouchi, "A methodology for implementation of high-efficiency broadband power amplifiers with second-harmonic manipulation," *IEEE Trans. Circuits Syst. II, Exp. Briefs*, vol. 63, no. 1, pp. 54–58, Jan. 2016.

[27] T. Sharma, R. Darraji, F. Ghannouchi, and N. Dawar, "Generalized continuous Class-F harmonic tuned power amplifiers," *IEEE Microw. Wireless Compon. Lett.*, vol. 26, no. 3, pp. 213–215, Mar. 2016.

[28] J. Chen, S. He, F. You, R. Tong, and R. Peng, "Design of broadband high-efficiency power amplifiers based on a series of continuous modes," *IEEE Microw. Wireless Compon. Lett.*, vol. 24, no. 9, pp. 631–633, Sep. 2014.

[29] G. L. Matthaei, "Design of wide-band (and narrow-band) band-pass microwave filters on the insertion loss basis," *IRE Trans. Microw. Theory Techn.*, vol. MTT-8, no. 6, pp. 580–593, Nov. 1960.

[30] M. S. Hashmi and F. M. Ghannouchi, "Introduction to load-pull systems and their applications," *IEEE Instrum. Meas. Mag.*, vol. 16, no. 1, pp. 30–36, Feb. 2013.

[31] W. Ku and W. Petersen, "Optimum gain-bandwidth limitations of transistor amplifiers as reactively constrained active two-port networks," *IEEE Trans. Circuits Syst.*, vol. 22, no. 6, pp. 523–533, Jun. 1975.

[32] O. Pitzalis and R. A. Gilson, "Broad-band microwave Class-C transistor amplifiers," *IEEE Trans. Microw. Theory Techn.*, vol. 21, no. 11, pp. 660–668, Nov. 1973.

[33] P. Saad, C. Fager, H. Cao, H. Zirath, and K. Andersson, "Design of a highly efficient 2–4-GHz octave bandwidth GaN-HEMT power amplifier," *IEEE Trans. Microw. Theory Techn.*, vol. 58, no. 7, pp. 1677–1685, Jul. 2010.

[34] J. C. Pedro, "The wonderful world of nonlinearity: A distinguished microwave lecture on the modeling and characterization of RF and microwave circuits," *IEEE Microw. Mag.*, vol. 16, no. 9, pp. 22–35, Oct. 2015.

[35] P. M. Cabral, J. C. Pedro, and N. B. Carvalho, "Nonlinear device model of microwave power GaN HEMTs for high power-amplifier design," *IEEE Trans. Microw. Theory Techn.*, vol. 52, no. 11, pp. 2585–2592, Nov. 2004.

[36] P. Aflaki, R. Negra, and F. M. Ghannouchi, "Intrinsic capacitances effects on the accuracy of the large-signal switch-based GaN device model," in *Proc. Asia Pacific Microw. Conf.*, Singapore, Dec. 2009, pp. 281–284.

[37] Y. Xu and R. Xu, "Compact modeling of GaN HEMTs for microwave high power amplifier design," in *Proc. IEEE Int. Conf. Commun. Problem-Solving*, Beijing, China, Dec. 2014, pp. 468–472.

[38] X. Zhao et al., "Temperature-dependent access resistances in large-signal modeling of millimeter-wave AlGaN/GaN HEMTs," *IEEE Trans. Microw. Theory Techn.*, vol. 65, no. 7, pp. 2271–2278, Jul. 2017.

[39] Nitronex Corp., "GaN for LDMOS users," Nitronex, Appl. Note 010, Jun. 2008. [Online]. Available: http://www.richardsonrfpd.com/resources/RellDocuments/SYS_16/Nitronex_GaN_for_LDMOS_Users_App%20Notes.pdf

[40] J. Moon, J. Kim, and B. Kim, "Investigation of a Class-J power amplifier with a nonlinear C_{out} for optimized operation," *IEEE Trans. Microw. Theory Techn.*, vol. 58, no. 11, pp. 2800–2811, Nov. 2010.

[41] B. Razavi, "Basic concepts in RF design," in *RF Microelectronics*, 2nd ed. Upper Saddle River, NJ, USA: Prentice-Hall, 2012, pp. 62–71.

XIANGYU MENG received the B.S. degree in electronic science and technology from Xidian University, Xi'an, China, in 2008, the M.S. degree in wireless communication and signal processing from the University of Bristol, U.K., in 2012, and the Ph.D. degree from the Beijing University of Posts and Telecommunication, in 2018.

He is currently a Technology Development Engineer with ZTE Corporation, China. His current research interests include broadband waveform engineering, high-efficiency broadband/dual-wideband RF PA design, and broadband transceiver architecture design.

CUIPING YU received the B.S. degree in communication engineering from Jilin University, Jilin, China, in 2004, and the Ph.D. degree in electronic engineering from the Beijing University of Posts and Telecommunications (BUPT), Beijing, China, in 2010.

Since 2013, she has been an Associate Professor with the School of Electronic Engineering, BUPT. Her research interests include nonlinear modeling and linearization of transmitters/power amplifiers, high efficiency power amplifiers design, and multi-band components design.

YUANAN LIU (M'93) received the B.S., M.S., and Ph.D. degrees in electrical engineering from the University of Electronic Science and Technology of China, Chengdu, China, in 1984, 1989, and 1992, respectively.

In 1984, he joined the 26th institute of Electronic Ministry of China to develop the inertia navigating system. In 1992, he began his first postdoctoral position with the EMC laboratory, Beijing University of Posts and Telecommunications (BUPT), Beijing, China. In 1995, he started his second postdoctoral position with the Broadband Mobile Laboratory, Department of System and Computer Engineering, Carleton University, Ottawa, Canada. Since 1997, he has been a Professor with the Wireless Communication Center, College of Telecommunication Engineering, BUPT, where he is involved in the development of next-generation cellular system, wireless LAN, Bluetooth application for data transmission, EMC design strategies for high speed digital system, and electromagnetic interference and electromagnetic susceptibility measuring sites with low cost and high performance. He is interested in smart antennas for high-capacity mobile signal processing techniques in fading environments, EMC for high-speed digital system, ISI suppression, orthogonal frequency division multiplexing (OFDM), and multicarrier system design. He is a Senior Member of the Electronic Institute of China.

YONGLE WU (M'12–SM'15) received the B.Eng. degree in communication engineering, and the Ph.D. degree in electronic engineering from the Beijing University of Posts and Telecommunications (BUPT), Beijing, China, in 2006 and 2011, respectively.

In 2010, he was a Research Assistant with the City University of Hong Kong, Hong Kong. In 2011, he joined BUPT, where he is currently a Full Professor with the School of Electronic Engineering. His research interests include microwave components, circuits, and antennas and wireless systems design.

XIYU WANG received the B.E. and M.S. degrees in electrification and automation of railway traction from Beijing Jiaotong University, Beijing, China, in 1998.

He has been working with ZTE Corporation, where he was involved in the research and innovation of wireless network technology, including key technologies such as CDMA IS95, CDMA 2000 1x/EVDO, ZXSDR soft base station platform, LTE, Pre5G, and so on.

JIANWEI WANG received the B.E. degree in electronic engineering from Xi'an Shiyou University, XiâĂŹan, China, in 2001, and the M.E. degree in information and communication engineering from the Beijing University of Posts and Telecommunications, Beijing, China, in 2009.

He is currently the Deputy Director of the National Key Laboratory of Mobile Networks and Mobile Multimedia. His research interests include the new generation wireless technology research with network architecture, RF and baseband systems, digital signal processing, key algorithms, and so on.

• • •